Disruption of photoautotrophic intertidal mats by filamentous fungi

Cátia Carreira[1,2*], Marc Staal[2], Daniel Falkoski[3], Ronald P. de Vries[3,4], Mathias Middelboe[2], Corina P.D. Brussaard[1,5]

[1] Department of Biological Oceanography, Royal Netherlands Institute for Sea Research (NIOZ), 8 PO Box 50, NL 1790, AB Den Burg, The Netherlands

[2] Section for Marine Biology, University of Copenhagen, Strandpromenaden 5, 3000 Helsingør, Denmark

[3] CBS-KNAW Fungal Biodiversity Centre, Utrecht, The Netherlands

[4] Fungal Molecular Physiology, Utrecht University, Utrecht, The Netherlands

[5] Aquatic Microbiology, Institute for Biodiversity and Ecosystem Dynamics, University of Amsterdam, Amsterdam, The Netherlands

[*]For correspondence. E-mail ccd.carreira@gmail.com; Tel. (+31) (0) 222369513; Fax (+31) (0) 222319674.

Running title: Fungus rings in photosynthetic microbial mats

Abstract

Ring-like structures, 2.0 - 4.8 cm in diameter, observed in photosynthetic microbial mats on the Wadden Sea island Schiermonnikoog (The Netherlands) showed to be the result of the fungus *Emericellopsis* sp. degrading the photoautotrophic top layer of the mat. The mats were predominantly composed of cyanobacteria and diatoms, with large densities of bacteria and viruses both in the top photosynthetic layer and in the underlying sediment. The fungal attack cleared the photosynthetic layer, however, no significant effect of the fungal lysis on the bacterial and viral abundances could be detected. Fungal mediated degradation of the major photoautotrophs could be reproduced by inoculation of non-infected mat with isolated *Emericellopsis* sp, and with an infected ring sector. Diatoms were the first re-colonisers followed closely by cyanobacteria that after about 5 days dominated the space. The study demonstrated that the fungus *Emericellopsis* sp. efficiently degraded a photoautotrophic microbial mat, with potential implications for mat community composition, spatial structure and productivity.

Introduction

Photosynthetic microbial mats, found worldwide in a variety of extreme environments (Castenholz, 1994), are dynamic laminated microbial communities containing photoautotrophs, micro fauna, fungi, heterotrophic bacteria, and viruses. The top layer of these mats is mostly composed of filamentous cyanobacteria and eukaryotic microalgae, which fuel the heterotrophic prokaryote communities inhabiting the underlying sediment (Van Gemerden, 1993; Canfield et al., 2005). Due to the reduced grazing activity (Fenchel, 1998) and the production of significant amounts of exopolymeric substances (EPS) by photoautotrophs and bacteria (De Brouwer et al., 2002), the mats often show a well defined laminated vertical structure. Under certain conditions, characterized by occasional flooding and low sand deposition, marine intertidal flats can sustain physical stable microbial mats (Stal, 1994). The chemical and biological landscapes of microbial mats are highly dynamic and the biomass and chemical gradients vary drastically on small spatial scales as well as in short time intervals. The chemical gradients are mainly driven by variable production and consumption rates within the mat and the biomass heterogeneity may be the result of variable growth conditions, local grazing and cell lysis caused by chemical compounds, fungi and viruses.

Fungi have previously been observed in hypersaline microbial mats (Cantrell et al., 2006), and in a recent study fungi were suggested to be diverse and quantitatively important components of carbon degradation in photosynthetic mats along with bacteria (Cantrell and Duval-Pérez, 2013). Furthermore it was shown that the fungal communities were more diverse in the oxic photosynthetic layer. Fungal activity may not be restricted to decomposition of detritus, as some fungi isolated from freshwater, soil and air have been

found to predate and lyse cyanobacteria and green algae (Safferman and Morris, 1962; Redhead and Wright, 1978; Redhead and Wright, 1980). Some of these fungi belonged to the genus A*cremonium* and *Emericellopsis* and produced a heat stable extracellular compound thought to be the antibiotic cephalosporin C. Furthermore parasitic microscopic fungi (chytrids) have been associated with bloom control of the diatom *Asterionella formosa* in both lakes (Canter and Lund, 1948) and culture studies (Bruning, 1991). Also, a bloom of the cyanobacteria *Anabaena macrospora* has been shown to be influenced by fungal predation (Gerphagnon et al., 2013). Despite the potential significance of fungi for the mortality and degradation of photoautotrophs, little is known about the ecological impact of benthic fungi in photosynthetic microbial mats.

Fairy-rings are a phenomenon occurring in terrestrial environments, where fungi grow in large radial shapes and may manifest as necrotic zones (Bonanomi et al., 2011; Caesar-TonThat et al., 2013; Ramond et al., 2014). To the best of our knowledge ring-structures caused by fungi have never been observed before in microbial mats. In the current study we investigated the spatial distribution of photoautotrophs, bacteria and viruses in ring-like structures that were found in intertidal photosynthetic microbial mats on the Wadden Sea island Schiermonnikoog (The Netherlands). These rings were caused by local cell lysis of filamentous cyanobacteria, caused by associated fungal activity.

Results

Ring-like structures were observed in the photosynthetic microbial mats on the island Schiermonnikoog (The Netherlands). These ring-like structures were examined by a

combination of autofluorescence imaging, epifluorescence microscopy and genomics in order to determine the cause of these patterns.

The horizontal distribution of photoautotrophs in the non-infected microbial mats was either characterized by a dominance of cyanobacteria or an equal mix of cyanobacteria and diatoms in both seasons, as showed by the blue to amber ratio (BAR) (fig. 1A, B). On average the BAR value was -0.4 ± 0.3, indicating the cyanobacterial dominance. The distribution of cyanobacteria and diatom populations was heterogeneous and the individual clusters were separated by mm distances.

Figure 1

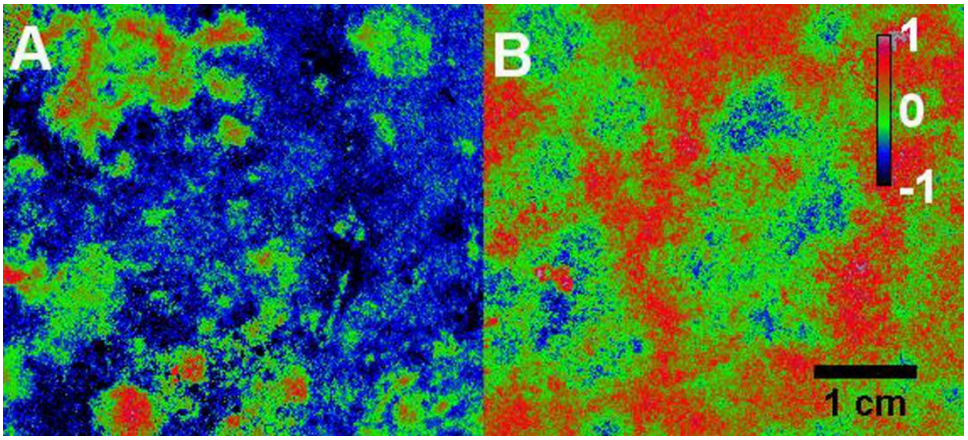

Ring-like structures (2.0 - 4.8 cm diameter) appeared in the photosynthetic microbial mats during summer and autumn (not observed during winter and spring). In November the microbial mat had been recently flooded (Fig. 2A, B). Whereas in July and August the mat was dry (Fig. 2C, D). To characterize the ring structures, distinct zones were identified. In November, two areas with different structure were identified: the ring core (“core”) and outside the ring (“outside”) (Fig. 3A). In July three distinct zones were identified in the ring structures: the ring core (“core”), the ring around the core (“ring”), and

outside the ring (“outside”). The “ring” area could usually be divided in two rings: “ring in” and “ring out” (Fig. 3A). In July control samples were also taken well away from ring (“mat”).

Figure 2

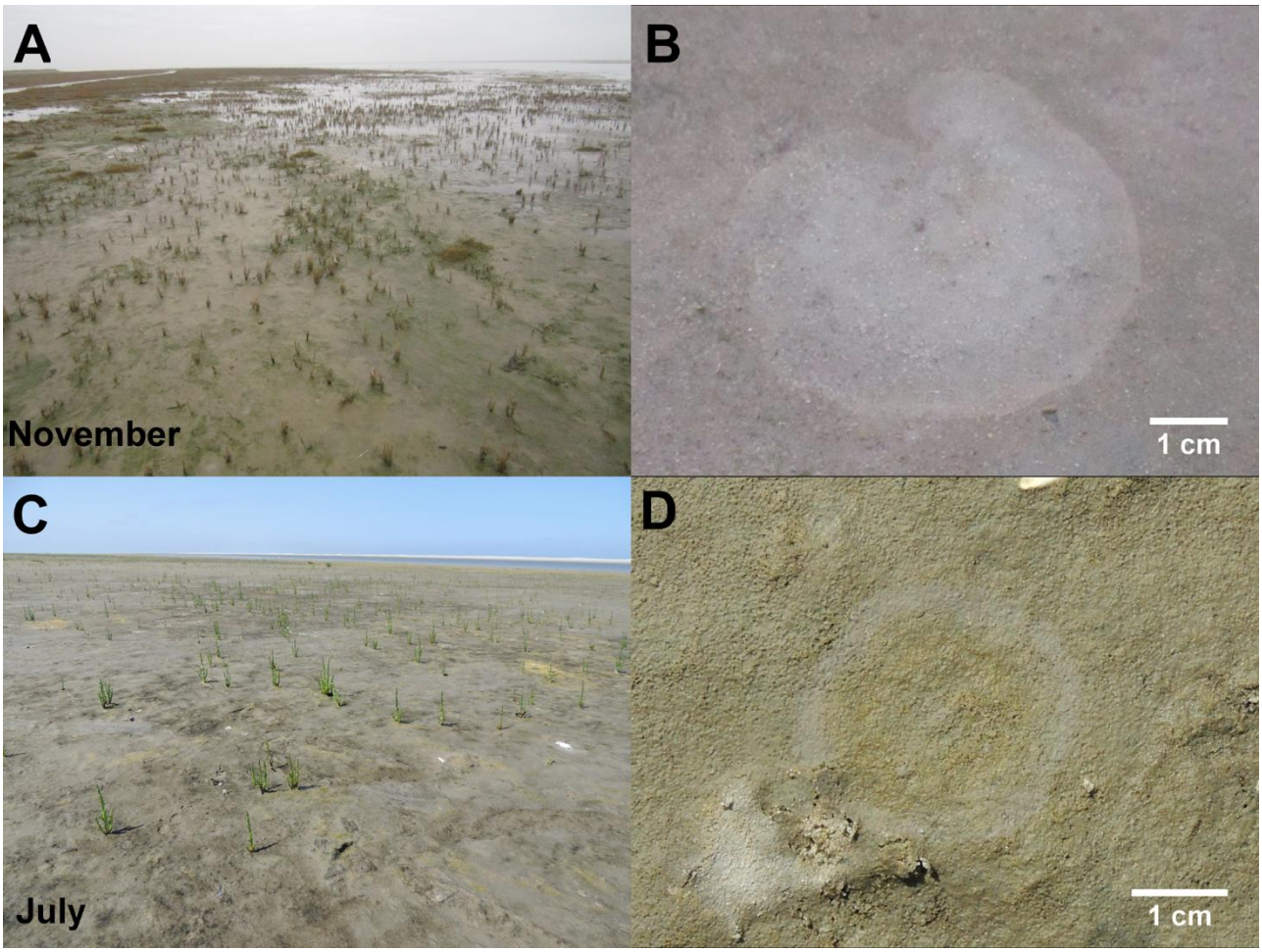

Examination of 5 rings by stereomicroscope and autofluorescence camera showed the “core” of the ring to be dominated by diatoms, with a minor share of cyanobacteria. The “ring in” was cleared of photoautotrophs, thus without autofluorescence, but white of colour. Fungal hyphae were observed in the “ring in” (Fig. 3). As the fungi spread towards the outside it formed another ring (“ring out”) with a light green colour. This ring contained some cyanobacteria filaments, although without autofluorescence, and a few fungal

111 hyphae (Fig. 3). The “outside” area was dark green in colour and similar to the control area

112 (“mat”) with a mix of cyanobacteria and diatom (Fig. 3E).

113

114 Figure 3

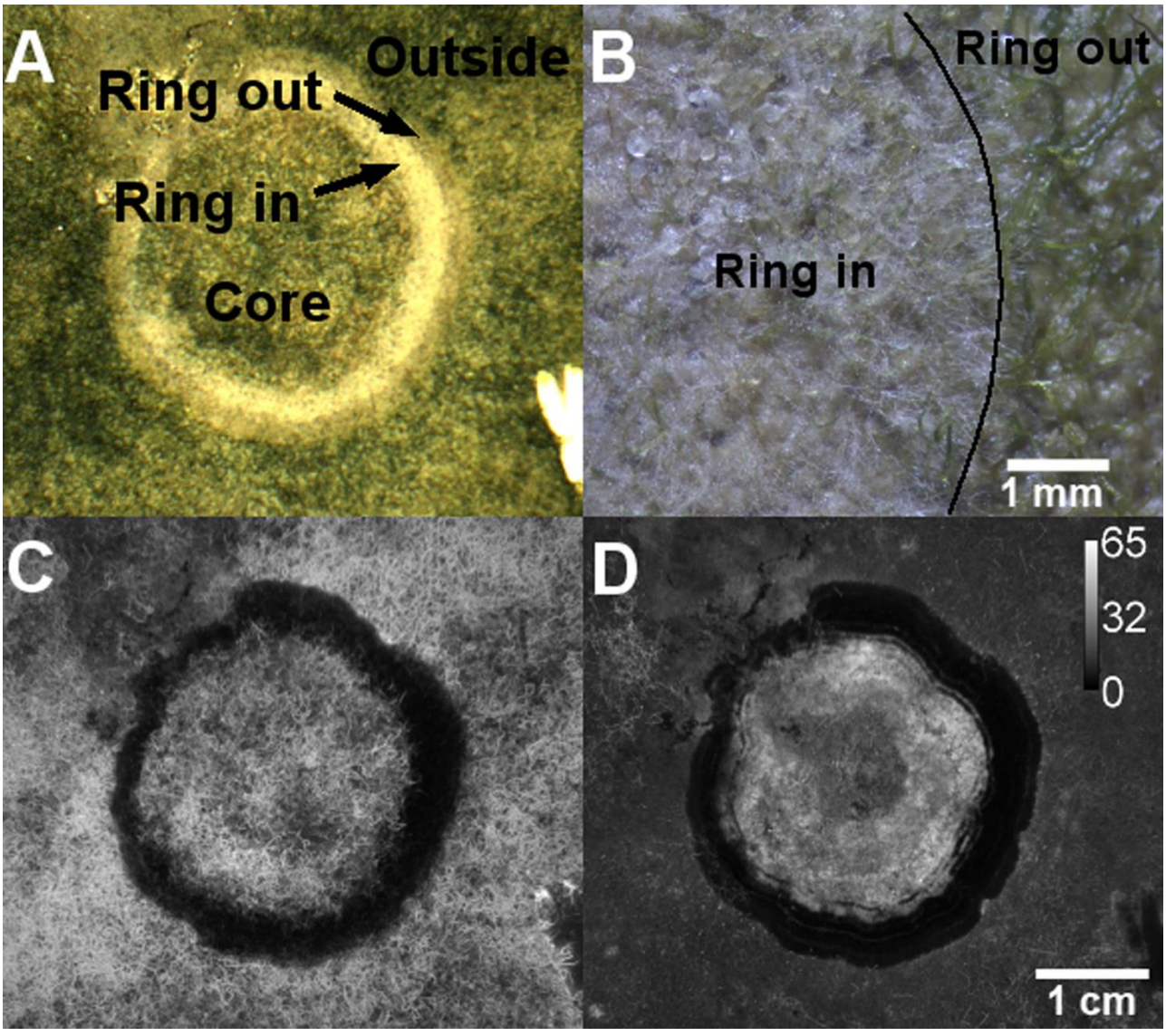

115

116 Figure 3E

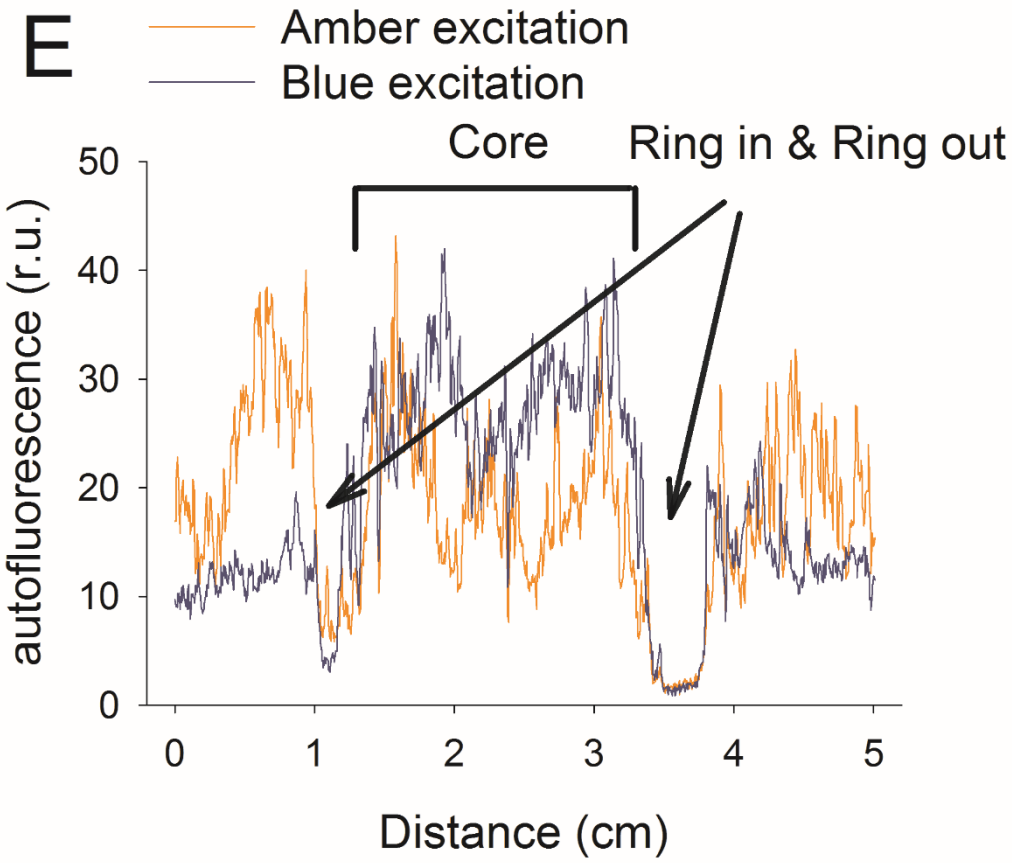
E
Amber excitation
Blue excitation
Core
Ring in & Ring out
autofluorescence (r.u.)
50
40
30
20
10
0
0
1
2
3
4
5
Distance (cm)

117

The bacterial abundances did not vary significantly across the different areas of the ring in any of the samples (Table 1). However the top layer always showed higher abundance than the bottom layer, in both seasons. While bacterial abundances in the top layer (0 - 1 mm) were similar in November and July (1.1 ± 0.4 $x10^{10}$ $g^{-1}$and 1.3 ± 0.4 x 10^{10} g^{-1}, respectively), the bottom layer (1 - 2 mm) showed a significantly ($p < 0.001$) lower bacterial abundance in July (0.4 ± 0.2 x 10^{10} g^{-1}) compared to November (0.9 ± 0.3 $x10^{10}$ g^{-1}). The total average bacterial abundances in November and July were similar, i.e.1.0 ± 0.4 x 10^{10} g^{-1} and 0.9 ± 0.5 x 10^{10} g^{-1}, respectively (Table 1).

As for the bacteria, viral abundances were similar in the different areas of the rings (Table 1). Viral abundances in both seasons were higher in the top layer (0 - 1 mm) than in the bottom layer (1 - 2 mm). In November the viral abundance in the 0 - 1 mm layer was similar (3.4 ± 1.2 x 10^{10} g^{-1}) to July (3.2 ± 1.2 x 10^{10} g^{-1}), but the bottom layer (0 - 2 mm) was 3-fold higher in November compared to July (8.5 ± 0.5 x 10^{10} g^{-1}; $p < 0.001$). The total viral abundance did not vary significantly over time and ranged from 2.1 ± 1.4 x 10^{10} g^{-1} (July) to 2.9 ± 1.3 x 10^{10} g^{-1}(November) (Table 1).

Virus to bacterium ratio (VBR) was not significantly different between the various ring areas. VBR in the bottom layer (1 - 2 mm) was generally lower than the top layer (Table 1) and significantly ($p < 0.05$) higher in November than in July for the 0 - 1 mm (3.0 ± 0.8 vs. 2.5 ± 0.7) and the 1 - 2 mm depth (2.8 ± 1.5 vs. 2.0 ± 0.4).

(Position of Table 1)

An examination of the fungal morphology and community composition was performed in July, revealing fungus threads in the “ring in” and “ring out” areas. Isolation of the fungi resulted in several colonies all with identical morphological characteristics, suggesting the presence of a single cultivable fungal species in the “ring in” and “ring out”.

142 Since all colonies showed the same characteristics, one unique fungal colony was
143 randomly chosen and subcultured several times to warrant a pure culture. The isolated
144 strain presented a radial growth with velvety and white hyphae. Microscopic examination
145 showed that hyphae were septated and hyaline. Sporulation was not observed even after
146 3 weeks of cultivation on MEA medium, indicating that the fungus requires specific
147 conditions to form reproductive structures.

148 Fungal identification was carried out by sequence analysis of three loci, LSU, ITS
149 and β-tubulin, and the sequences obtained have been deposited in GenBank database
150 (Accession number: KJ196387, KJ196386 and KJ196385, respectively). A phylogenetic
151 analysis was performed comparing the obtained sequences to available sequences of
152 species of the genus *Acremonium* and *Emericellopsis*. As a first step a one-gene analysis
153 was performed using the LSU sequence, determining the phylogenetic position of the
154 isolated strain in the *Acremonium* clade belonging to the order Hypocreales (Summerbell
155 et al., 2011). The phylogenetic tree 1 (see Fig. S1) demonstrated that the isolated strain
156 falls into the *Emericellopsis* clade (94% bootstrap support), which includes species such
157 as *Acremonium exuviaruam, Acremonium salmoneum, Acremonium potronii and*
158 *Acremonium tubakii.* A second phylogenetic analysis was performed focussing on the
159 *Emericellopsis* clade using a two-gene analysis based on the ITS and β-tub sequences
160 and the dataset generated by Grum-Grzhimaylo et al. (2013). This study suggested that
161 the *Emericellopsis* clade could be split into a terrestrial clade, a marine clade and an
162 alkaline soil clade. The phylogenetic tree (Fig. 4) indicated that the fungal strain isolated
163 from “ring in” fell into the terrestrial clade. The strain was most closely related to
164 *Emericellopsis terricola*, *Emericellopsis microspora*, *Emericellopsis robusta* and

165 *Acremonium tubakii*. Based on this analysis we classified the strain isolated from “ring in”

166 as *Emericellopsis* sp. CBS 137197.

167

168 Figure 4

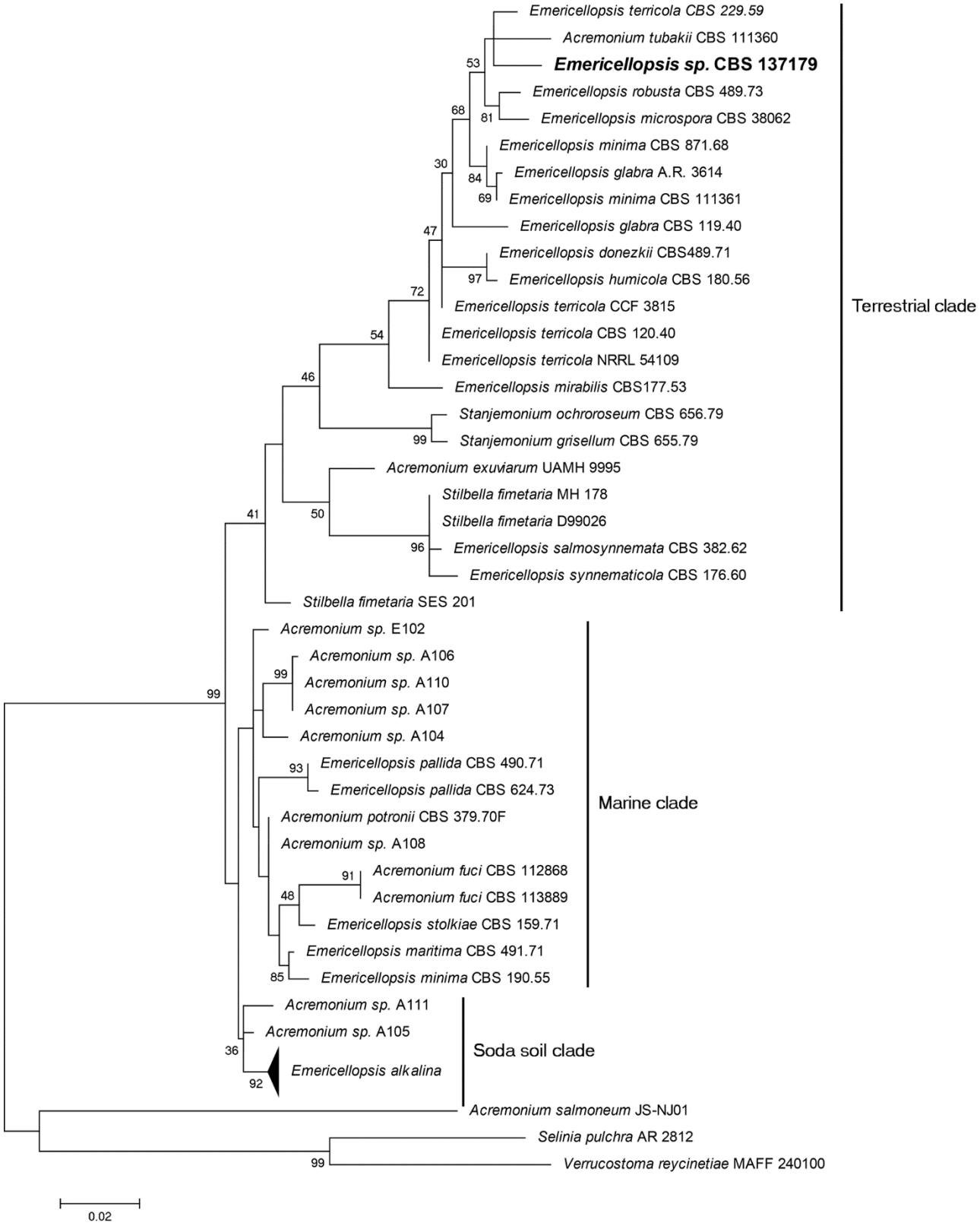

Samples of healthy mat were inoculated with the isolated strain *Emericellopsis sp.* CBS 137197 (mycelium fragments) aiming to confirm the fungus as the specific causative

for the degradation of the photoautotrophic layers. Autoclaved mycelium was used as a negative control in this experiment. The healthy mat showed rings development already after 3 days in all replicates (n = 20), with similar morphology as the natural ring-structures observed in the mats. *Emericellopsis* sp. cleared the infection zone, showing no autofluorescence for cyanobacteria and diatom, and expanding outside while degrading the mat community at an average speed of 0.06 ± 0.01 cm d^{-1} (varied between 0.05 and 0.07 ± 0.01 cm d^{-1}). The total area degraded per ring during the inoculation experiment ranged between 0.5 to 1.3 cm^2. Addition of killed (autoclaved) mycelium of *Emericellopsis* sp. did not result in ring structures (n = 17, Fig. 5).

Figure 5

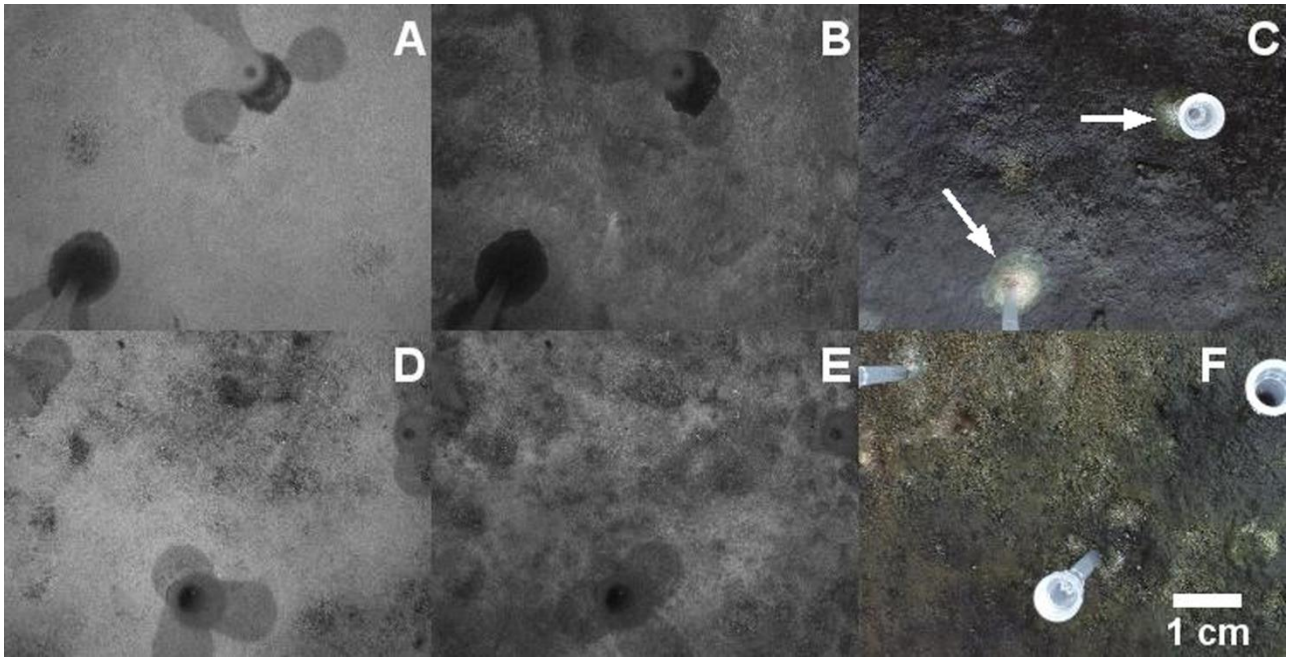

The fungal induced lysis of the photoautotrophs and the subsequent re-colonization of the main photoautotrophs was demonstrated by transferring a piece of microbial mat infected with fungus (“ring in” and “ring out”) to a non-infected microbial mat. The results showed that the fungi in the “ring” area were able to degrade the photoautotrophs (Fig. 6).

The fungi moved from the transplanted area into the new mat while leaving a trail of cleared mat with no autofluorescence (for both cyanobacteria and diatom). This cleared zone was then re-colonised first by diatoms, showing a strong autofluorescence after blue light excitation, and subsequently, after about 5 days, cyanobacteria showed increasing autofluorescence in the same area (Fig. 6).

Figure 6

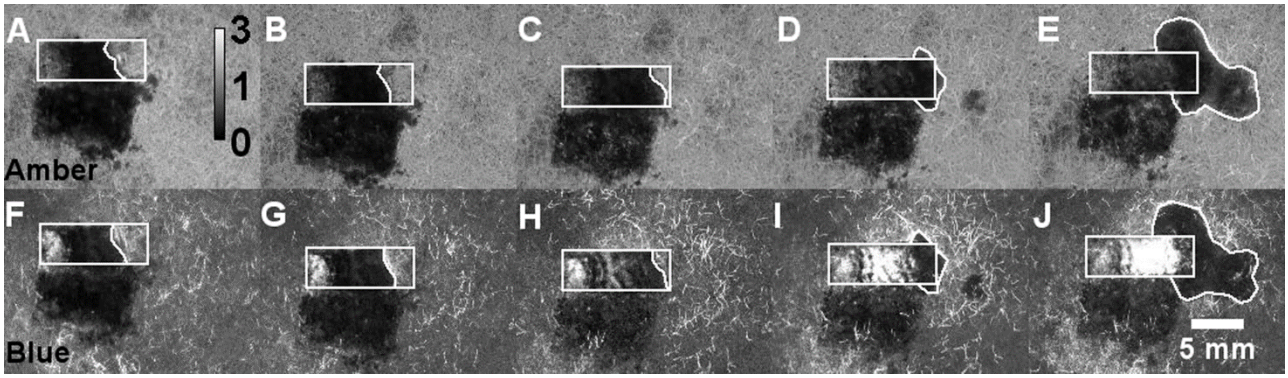

The “ring out” area, without autofluorescence, contained fewer fungi than observed in the “ring in” area. In the “core”, “outside” and the “mat” areas the microbial mat did not show visible fungi. The temporal development of the rings due to fungal attack was recorded and measured over a 10 days period by colour and autofluorescence imaging (Fig. 7). Autofluorescence images after amber and blue light excitation showed the growth of cyanobacteria and diatoms, respectively, compared to day 0. All 8 rings collected and analysed in November and July were about 2 to 4.8 cm wide, and expanded at an average rate of 0.12 ± 0.01 cm d^{-1} (Table 2). The oxygenic photoautotrophic re-growth, however, was slower (0.04 - 0.07 cm d^{-1} for cyanobacteria, and 0.07 - 0.09 cm d^{-1} for diatoms). Despite expected differences in environmental conditions and/or amount of fungus, the range in degradation rates for these natural rings (Table 2) as well as the inoculation

experiments (Fig. 5) is relatively small (0.05-0.17 cm d^{-1}). We estimated that these ring patterns occupied up to 10 % of the microbial mat surface area in the area studied (see Fig. S2). The total beach area where we found these ring structures was about 800 x 30 m. Furthermore, we observed different regions, i.e. (i) with clear ring coverings like described here, (ii) with bigger infected regions, likely representing older infection stages but still with sharp edges of infection, and (iii) with rings grown together (Fig. S2).

(Position of Table 2)

Figure 7

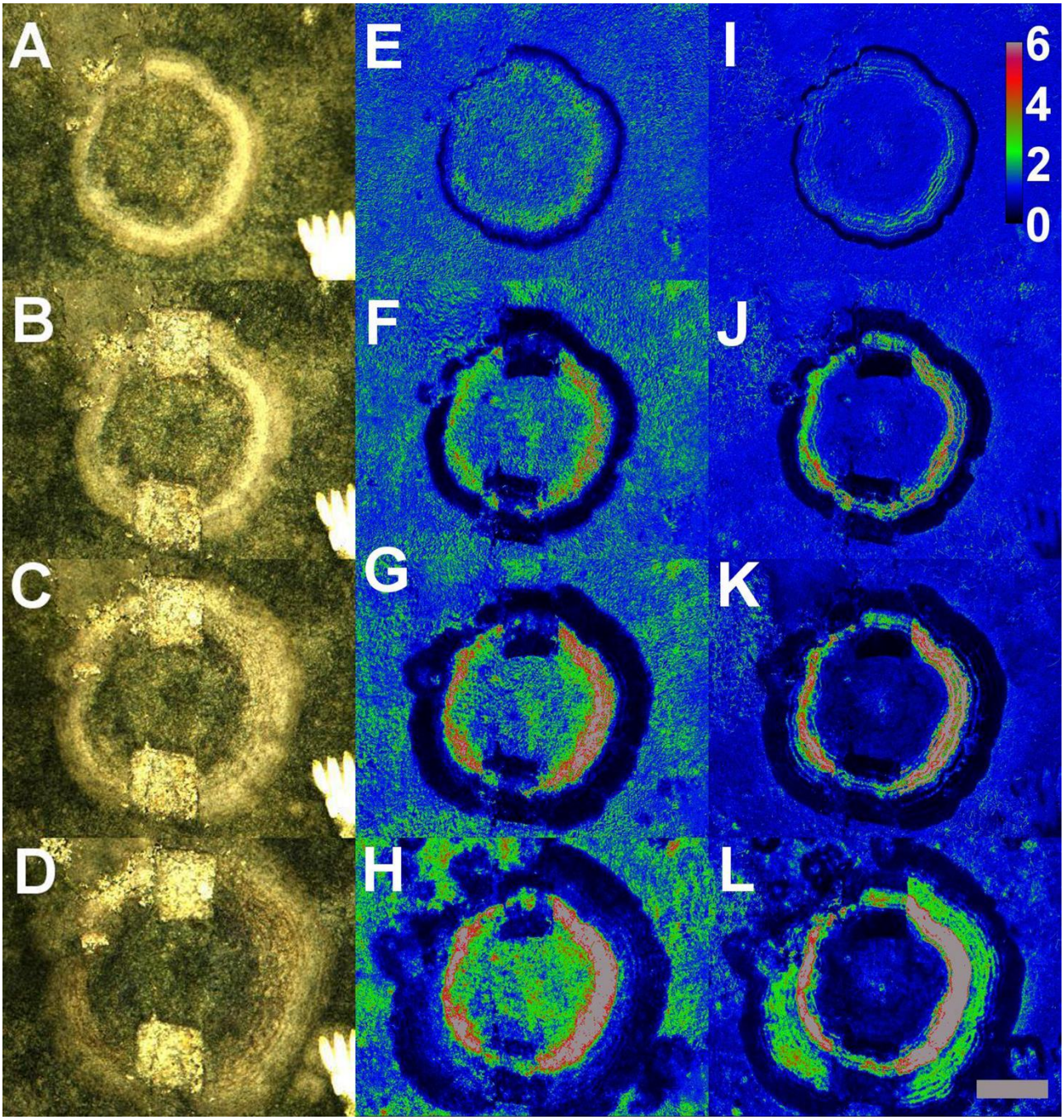

Discussion

Examination of the ring-like structures and development over time showed clearly that the fungus *Emericellopsis* sp. CBS 137197 efficiently degraded the photoautotrophs in the microbial mats, leaving a clear zone of lysed cells. Despite the presence of this fungus

223 in a marine environment, phylogenetic analysis showed that the fungus falls within the
224 terrestrial *Emericellopsis* clade. However, other strains belonging to *Emericellopsis*
225 terrestrial clade have also been isolated from aquatic environments, such as *E. donezkii*
226 CBS 489.71, *E. minima* CBS111361 and *A. tubakii* CBS 111360 (Grum-Grzhimaylo et al.,
227 2013). Even *E. terricola*, a member of the terrestrial clade and representative of a
228 commonly collected species with known marine habitat associations, could undergo
229 conidial germination and growth in sea water (Zuccaro et al., 2004). These examples
230 suggest that some fungi belonging to *Emericellsopsis* clade present remarkable adaptive
231 properties and are able to live in both terrestrial and marine biotopes. Fungi are known to
232 control algal blooms in freshwater (Canter and Lund, 1948; Kagami et al., 2006), infect
233 marine phytoplankton (Park et al., 2004; Wang and Johnson, 2009) and have also been
234 observed in more extreme marine systems such as deep sea hydrothermal systems and
235 hypersaline microbial mats (Le Calvez et al., 2009; Cantrell and Duval-Pérez, 2013).
236 The different areas of the ring structure showed a clear temporal development, with
237 *Emericellopsis* sp. moving from the initial central core towards the outside in a circular
238 shape, thus leaving a trail of recognisable patterns. *Emericellopsis* sp. initially feeds on
239 photoautotrophs (“ring in”) and at the same time moves towards non-infected mat (“ring
240 out”) for new supply of resources. This could be facilitated by the release of e.g. toxins or
241 enzymatic activity diffusing out from the fungi, thus creating the characteristic periphery of
242 the ring (“ring out”). The actual mechanism of cell lysis remains unknown. *Emericellopsis*
243 sp. fungal species have been shown to produce the antibiotic Cephalosporin C that lysed
244 cyanobacteria (Redhead and Wright, 1978). Quickly after the fungi cleared the mat from
245 photoautotrophs, a re-colonisation process took place with diatoms appearing first and

246 cyanobacteria following a few days later and finally dominating the mat again (see
247 schematics in Fig. 8).

248 Figure 8

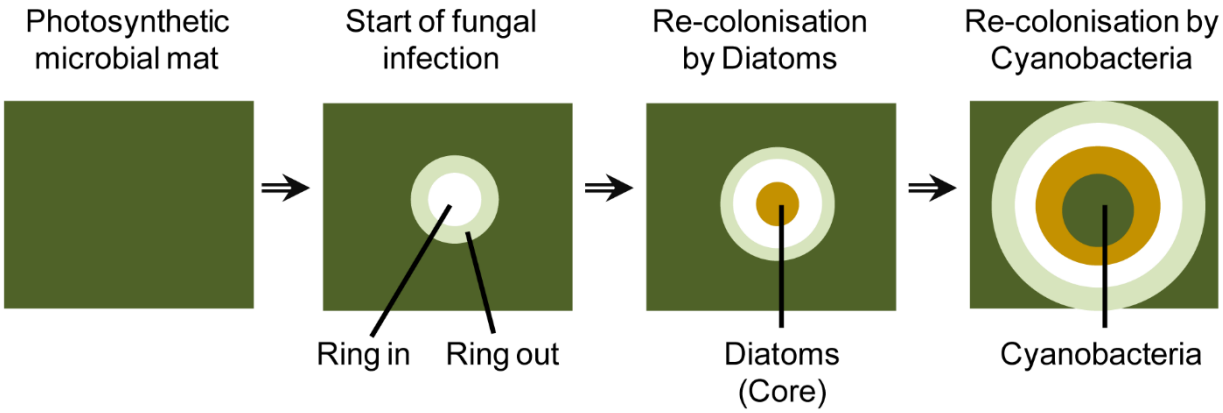

249

250

251 It is currently unclear whether the re-colonisation was initiated by the same species
252 (new entry or emerged from deeper subsurface layer) as before the fungal attack, or
253 whether new, perhaps toxin-resistant photoautotrophs colonised the area. As fungi were
254 not observed in the core of the ring following lysis, it is likely that their potential toxic effect
255 has disappeared, thus allowing the same algae to re-colonize the area again. The newly
256 colonised areas with diatoms showed higher autofluorescence compared to outside ring
257 reference mat. Single celled diatoms are known to move fast in sediments (Harper, 1969),
258 thus under fungal attack, we speculate that they may have escaped fungal lysis by
259 migrating downwards. Filamentous cyanobacteria glide slower than diatoms (Watermann
260 et al., 1999 and references therein), thus probably becoming trapped in the fungal hyphae,
261 or dying from toxin release. As the fungi moved away from the original attack area,
262 diatoms would re-surface and thrive temporarily without the competing cyanobacteria
263 present.

The direct impact of the fungi on photoautotrophic degradation of the mats may also have implications for the cycling of organic matter and nutrients within the mats as fungi have been shown to release labile organic matter and nutrients during degradation of refractory matter (Sigee, 2005). Possibly, algal lysate and other organic matter remnants from the fungal degradation support bacterial and viral production in the cleared zones. Overall, the potential increased heterotrophic activity could stimulate the remineralisation of inorganic nutrients sustaining the new photoautotrophic production in the mats. Consequently, fungal infections probably drive a local regenerated production that may increase the overall productivity of the mat. The reduction of photoautotrophic biomass due to fungal degradation, however, was not reflected in increased bacterial and viral abundances in the infected sections (“ring in” and “ring out”) compared to the non-infected areas (“core”, “outside”, and “mat”). This suggested that the lysed photoautotrophic cells were efficiently utilized by the fungi or alternatively, that increased bacterial activity did not result in enhanced net abundance. However, more sensitive methods for estimating bacterial activity should be applied in future studies to investigate a possible association between the distribution and activity of fungi and bacteria.

The rings in November did not show the “ring in” and “ring out” areas compared to July. This could simply reflect that the finer details of the ring structures could not be visually resolved in the more wet sediment in November, although a different type of fungal infection, with different ring morphology, cannot be ruled out. Cantrell et al. (2006) isolated 16 different fungal species from a hypersaline microbial mat, suggesting that fungi are a common feature of microbial mats potentially involved in mat lysis. Nevertheless, we show that *Emericellopsis* sp. was isolated and identified in these mats in two consecutive years. Further study is needed to clarify if also other fungi can cause ring structures and what the

exact underlying mechanism is. The ring structures were only found during summer and autumn, suggesting that low temperature and photoautotroph biomass limit fungal activity during winter and spring. Gerdes (2007) speculated that other ring-structures (although bigger in diameter) found in microbial mats, may result from gas surfacing from small exit points in the mat causing dispersal of nutrients and stimulation of cyanobacterial growth, although no conclusive studies were followed.

In summary, we showed that a fungus belonging to the *Emericellopsis* clade was able to clear photoautotrophs in benthic microbial mats by degradation, resulting in a series of characteristic ring-shaped patterns in the microbial mats, alike smaller versions of necrotic fairy-rings observed in terrestrial systems (e.g. Caesar-TonThat et al., 2013). The structures were observed during 4 consecutive years (3 of which were sampled) indicating that this is a common feature in intertidal photosynthetic microbial mats. The impact of the fungal lysis of the mat, did not, however, significantly affect the abundance or distribution of bacteria and viruses. This loss factor of cyanobacteria and diatoms seems to constitute an important mortality factor for photosynthetic microbial mats, with implications for mat community composition, productivity and spatial structure.

Experimental Procedures

Sampling

Intertidal photosynthetic microbial mat samples were collected during autumn (November 2012) and summer (July 2013 and August 2014) from the island Schiermonnikoog, situated in the intertidal Wadden Sea, The Netherlands (53° 29'

24.29"N, 6° 8' 18.02"E). Microbial mats with visible ring structures were cut out of the mat structure and placed inside a box (15 x 8 x 4 cm; L x W x H). The samples were transported back to the laboratory within 3 - 4h after sampling, where they were kept outside, at *in situ* conditions until use.

Chlorophyll quantification

Chlorophyll autofluorescence images were taken every second day for 10 days to see whether there were changes in the rings over time. The images were obtained according to Carreira et al. (2015b). Briefly, photographs were taken using a cooled CCD 16 bits camera (Tucsen Imaging Technology Co. LTD, China) (1360 x 1024), with a long pass 685 nm filter placed in front of the camera. The microbial mats were exposed to blue and amber light excitation, to distinguish between diatoms and cyanobacteria, respectively. Images were analysed with Image J (1.47m). Autofluorescence images of blue to amber (BAR) were used as an indicator of cyanobacteria dominance (< 0), or diatoms dominance (> 0). Colour images were also taken using a 12 bits CCD colour camera (Basler Scout, Germany), and in July, images of the fungus were obtained by stereomicroscope (Carl Zeiss, Germany).

Viral and bacterial abundances

For enumeration of bacteria and viruses, samples of 1 x 0.5 x 0.1 cm (L x W x H) were taken from distinct locations in the ring, at two depths (0 - 1 and 1 - 2 mm). In November samples were taken to the “core” and “outside”, in a total of three samples per

area per ring, in 4 rings. In July samples were taken to “core”, “ring in”, “ring out”, “outside”, and to “mat” (control). Two samples were collected per area and per ring in a total of 3 rings.

Extraction of bacteria and viruses were done according to Carreira et al. (2015a). Briefly, the samples were placed in sterile 2 mL Eppendorf tubes and fixed with 2 % glutaraldehyde final concentration (25 % EM-grade, Merck) for 15 min at 4ºC, after which samples were incubated with 0.1 mM EDTA (final concentration) on ice and in the dark for another 15 min. Thereafter probe ultrasonication (Soniprep 150; 50 Hz, 4 µm amplitude, exponential probe) was applied in 3x cycles of 10 sec with 10 sec intervals, while keeping the samples in ice-water. Then 1 µL subsample was diluted in 1 mL of sterile MilliQ water (18 Ω) with 1 µL of Benzonase Endonuclease from *Serratia marcescens* (Sigma-Aldrich**;** > 250 U μL^{-1}**)** and incubated in the dark at 37ºC for 30 min. Next the samples were placed on ice until filtration. Each sample was filtered onto a 0.02 µm pore size (Anodisc 25, Whatman) and stained according to Noble & Fuhrman (1998) using SYBR Gold (Molecular Probes®, Invitrogen Inc., Life Technologies™, NY, USA). The filter was rinsed three times with sterile MilliQ after which it was mounted on a glass slide with an anti-fade solution containing 50 % glycerol, 50 % phosphate buffered solution (PBS, 0.05 M Na_2HPO_4, 0.85 % NaCl, pH 7.5) and 1 % *p*-phenylenediamine (Sigma-Aldrich, The Netherlands) and stored at -20ºC. Viruses and bacteria were counted using a Zeiss Axiophot epifluorescence microscope at x1150 magnification. At least 10 fields and 400 viruses and bacteria each were counted per sample.

Fungal isolation and identification

An isolation procedure was carried out intending to identify the fungal agents involved in the formation of the ring structure on the intertidal photosynthetic microbial mat. A mat sample (15 x 8 x 4 cm; L x W x H) containing several ring structures was collected as previous described and the presence of fungi on this structure was investigated. Ten pieces (0.5 x 0.5 x 0.1 cm; L x W x H) of mat were randomly taken from the “ring in” in different rings and transferred to a tube containing 10 mL of sterilized water. This mixture was vigorously stirred for 2 minutes and afterwards 100 µL of this suspension was used to inoculate malt extract agar (MEA) plates supplemented with penicillin and streptomycin to avoid bacterial growth. After 7 days of incubation at 25°C fungal colonies were observed on all plates. A unique fungal colony was randomly chosen and sub cultured several times in Petri dishes to ensure the obtainment of a pure culture.

Fungal identification was carried out by amplification and sequencing of three nuclear loci including LSU (large subunit of the nuclear ribosomal RNA gene), ITS (including internal transcribed spacer regions 1 and 2, and the 5.8S rRNA regions of the nuclear ribosomal RNA gene cluster) and β-tub (beta-tubulin intron 3).

Fungal genomic DNA of the isolated strain was isolated using the FastDNA® Kit (Bio 101, Carlsbad, USA) according to the manufacturer’s instructions. A fragment containing the LSU region was amplified using primers NL1 (GCATATCAATAAGCGGAGGAAAAG) (O’Donnell, 1996) and LR5 (ATCCTGAGGGAAACTTC) (Vigalys and Hester, 1990). A fragment containing the ITS region was amplified using forward primer ITS5 (GGAAGTAAAAGTCGTAACAAGG) and reverse primer ITS4 (TCCTCCGCTTATTGATATGC) (White et al., 1990). The β-tub fragment was amplified using primers Bt2a (GGTAACCAAATCGGTGCTGCTTTC) and Bt2b (ACCCTCAGTGTAGTGACCCTTGGC) (Glass and Donaldson, 1995). PCR and

sequencing procedures were performed as described previously by Summerbell et al. (2011).

The amplified sequences were compared with homologous sequences deposited in Genbank database and Maximum Likelihood phylogenetic trees were constructed using MEGA 5.0. Maximum parsimony analysis was performed for all datasets using the heuristic search option. The robustness of the most parsimonious trees was evaluated with 1000 bootstrap replications.

The procedure for fungal isolation and identification described above was repeated with mat samples collected in August 2014 and the fungal strain obtained in this second isolating process was absolutely, morphologically and genetically, related with the strain *Emericellopsis sp*. 137197 isolated in the year before.

Healthy mat samples were inoculated with *Emericellopsis* sp 137197 to confirm its ability to attach and degrade photoautotrophic microbial mats. The fungus was cultivated in liquid media with the following composition ($g.L^{-1}$): $NaNO_3$ 6,0; KH_2PO_4 1,5; KCl 0,5; $MgSO_4$ 0,5; glucose 10 and 200 µL of trace solution (EDTA 1.0%; $ZnSO_4.7H_2O$ 0.44%; $MnCl_2.4H_2O$ 0.1%; $CoCl_2.6H_2O$ 0.032%; $CuSO_4.5H_2O$ 0.031%; $(NH_4)_6Mo_7O_{24}.4H_2O$ 0.022%; $CaCl_2$. $2H_2O$ 0.15%; $FeSO_4.7H_2O$ 0.1%). The cultivation was carried out for 3 days in orbital shaker at 25 °C and 200 rpm. The broth containing the mycelial biomass was homogenized in a blender and directly employed for inoculation. A micropipette was employed to inoculate the mat and 50 µL of homogenized broth were applied in each spot test (n = 20). A negative control (killed fungus) was carried out in parallel by inoculation of healthy mat with autoclaved homogenized broth (120 °C, 20 min) (n = 17). All samples were incubated outside at ambient temperature to mimic, as close as possible, natural

conditions. The development of ring-like structures was followed over 10 days by autofluorescence and colour images.

To examine the effect of the fungus as the degrading agent of the mat and for the development of the ring structures in the photoautotrophs, a piece (1 x 0.5 x 0.1 cm; L x W x H) of microbial mat containing “ring in”, “ring out”, and “outside” was transplanted into a non-infected microbial mat. The growth was followed with autofluorescence images taken every day for 7 days.

Statistical analyses

To determine differences in viral and bacterial abundances, and VBR between seasons, depths, and sampled areas, ANOVA with post hoc Tukey HSD tests were performed. Prior to statistical analysis, normality was checked and the confidence level was set at 95 %. All statistical analysis was conducted in SigmaPlot 12.0.

Acknowledgments

The study received financial support from Fundação para a Ciência e a Tecnologia (FCT) – SFRH/BD/43308/2008, The Royal Netherlands Institute for Sea Research (NIOZ), Conselho Nacional de Pesquisa e Desenvolvimento Científico (CNPq), and the Danish Research Council for Independent Research (FNU). We thank Christian Lønborg, Tim Piel and Robin van de Ven, and Kirsten Kooijman for field and laboratory assistance. We also thank two anonymous reviewers for their constructive comments on the manuscript.

References

Bonanomi, G., Mingo, A., Incerti, G., Mazzoleni, S., and Allegrezza, M. (2011) Fairy rings caused by a killer fungus foster plant diversity in species-rich grassland. *J Veg Sci* **23**: 236-248.

Bruning, K. (1991) Infection of the diatom *Asterionella* by a chytrid. I. Effects of light on reproduction and infectivity of the parasite. *J Plankton Res* **13**: 103-117.

Caesar-TonThat, T.C., Espeland, E., Caesar, A.J., Sainju, U.M., Lartey, R.T., and Gaskin, J.F. (2013) Effects of *Agaricus lilaceps* fairy rings on soil aggregation and microbial community structure in relation to growth stimulation of western wheatgrass (*Pascopyrum smithii*) in Eastern Montana Rangeland. *Microb Ecol* **66**: 120-131.

Canfield, D.E., Thamdrup, B., and Kristensen, E. (2005) *Aquatic Geomicrobiology*. Amsterdam: Elsevier Academic Press.

Canter, H.M., and Lund, J.W.G. (1948) Studies on plankton parasites I. fluctuations in the numbers of *Asterionella formosa* Hass. in relation to fungal epidemics. *New Phytol* **47**: 238-261.

Cantrell, S.A., and Duval-Pérez, L. (2013) Microbial mats: an ecological niche for fungi. *Front Microbiol* **3**: 424.

Cantrell, S.A., Casillas-Martínez, L., and Molina, M. (2006) Characterization of fungi from hypersaline environments of solar salterns using morphological and molecular techniques. *Mycol Res* **110**: 962-970.

Carreira, C., Staal, M., Middelboe, M., and Brussaard, C.P.D. (2015a) Counting viruses and bacteria in photosynthetic microbial mats. *Appl Environ Microbiol* **81**: 10.1128/AEM.02863-02814

Carreira, C., Staal, M., Middelboe, M., and Brussaard, C.P.D. (2015b) Autofluorescence imaging system to discriminate and quantify the distribution of benthic cyanobacterial and diatom. *Limnol Oceanogr Methods*: in press.

Castenholz, R.W. (1994) Microbial mat research: the recent past and new perspectives. In *Proceedings of the NATO advanced research workshop on structure, development and environment significance of microbial mats*. Stal, L.J., and Caumette, P. (eds). Arcachon, France: Springer-Verlag, pp. 3-18.

De Brouwer, J.F.C., Ruddy, G.K., Jones, T.E.R., and Stal, L.J. (2002) Sorption of EPS to sediment particles and the effect on the rheology of sediment slurries. *Biogeochemistry* **61**: 57-71.

Fenchel, T. (1998) Formation of laminated cyanobacterial mats in the absence of benthic fauna. *Aquat Microb Ecol* **14**: 235-240.

Gerdes, G. (2007) Structures left by modern microbial mats in their host sediment. In *Atlas of microbial mat features preserved within the clastic rock record*. Schieber, J., Bose, P.K., Eriksson, P.G., Banerjee, S., Sarkar, S., Altermann, W., and Catuneau, O. (eds): Elsevier, pp. 5-38.

Gerphagnon, M., Latour, D., Colombet, J., and Sime-Ngando, T. (2013) Fungal parasitism: life cycle, dynamics and impact on cyanobacterial blooms. *PLoS ONE* **8**: e60894.

Glass, N.L., and Donaldson, G.C. (1995) Development of primer sets designed for use with the PCR to amplify conserved genes from filamentous Ascomycetes. *Appl Environ Microbiol* **61**: 1323–1330.

Grum-Grzhimaylo, A.A., Georgieva, M.L., Debets, A.J.M., and Bilanenko, E.N. (2013) Are alkalitolerant fungi of the *Emericellopsis* lineage (Bionectriaceae) of marine origin? *IMA Fungus* **4**: 213-228.
Harper, M.A. (1969) Movement and migration of diatoms on sand grains. *Brit Phycol J* **4**: 97-103.
Kagami, M., Gurung, T.B., Yoshida, T., and Urabe, J. (2006) To sink or to be lysed? Contrasting fate of two large phytoplankton species in Lake Biwa. *Limnol Oceanogr* **51**: 2776-2786.
Le Calvez, T., Burgaud, G., Mahe, S., Barbier, G., and Vandenkoornhuyse, P. (2009) Fungal diversity in deep-sea hydrothermal ecosystems. *Appl Environ Microbiol* **75**: 6415-6421.
Noble, R.T., and Fuhrman, J.A. (1998) Use of SYBR Green I for rapid epifluorescence counts of marine viruses and bacteria. *Aquat Microb Ecol* **14**: 113-118.
O'Donnell, K. (1996) Progress towards a phylogenetic classification of Fusarium. *Sydowia* **48**: 57-70.
Park, M.G., Yih, W., and Coats, D.W. (2004) Parasites and phytoplankton, with special emphasis on dinoflagellate infections. *J Eukaryot Microbiol* **51**: 145-155.
Ramond, J.-B., Pienaar, A., Armstrong, A., Seely, M., and Cowan, D.A. (2014) Niche-partitioning of edaphic microbial communities in the Namib Desert gravel plain fairy circles. *PLoS ONE* **9**: e109539.
Redhead, K., and Wright, S.J. (1978) Isolation and properties of fungi that lyse blue-green algae. *Appl Environ Microbiol* **35**: 962-969.
Redhead, K., and Wright, S.J.L. (1980) Lysis of the cyanobacterium *Anabaena flos-aquae* by antibiotic-producing fungi. *J Gen Microbiol* **119**: 95-101.
Safferman, R.S., and Morris, M.-E. (1962) Evaluation of natural products for algicidal properties. *Appl Microbiol* **10**: 280-292.
Sigee, D.C. (2005) Fungi and fungal-like organisms: aquatic biota with a mycelial growth form. In *Freshwater microbiology, biodiversity and dynamic interactions of microorganisms in the aquatic environment*: John Wiley & Sons, LTD, p. 544.
Stal, L.J. (1994) Microbial mats in coastal environments. In *Proceedings of the NATO advanced research workshop on structure, development and environment significance of microbial mats*. Stal, L.J., and Caumette, P. (eds). Arcachon, France: Springer-Verlag, pp. 21-32.
Summerbell, R.C., Gueidan, C., Schroers, H.J., Hoog, G.S., Starink, M., Rosete, Y.A. et al. (2011) *Acremonium* phylogenetic overview and revision of *Gliomastix*, *Sarocladium*, and *Trichothecium*. *Stud Mycol* **68**: 139-162.
Van Gemerden, H. (1993) Microbial mats: a joint venture. *Mar Geol* **113**: 3-25.
Vigalys, R., and Hester, M. (1990) Rapid genetic identification and mapping of enzymatically amplified ribosomal DNA from several *Cryptococcous* species. *J Bacteriol* **172**: 4238-4246.
Wang, G., and Johnson, Z.I. (2009) Impact of parasitic fungi on the diversity and functional ecology of marine phytoplankton. In *Marine Phytoplankton*. Kersey, W.T., and Munger, S.P. (eds): Nova Science Publishers, Inc., pp. 211-228.
Watermann, F., Hillebrand, H., Gerdes, G., Kumbein, W.E., and Sommer, U. (1999) Competition between benthic cyanobacteria and diatoms as influenced by different grain sizes and temperatures. *Mar Ecol Prog Ser* **187**: 77-87.

White, T.J., Bruns, T., Lee, S., and Taylor, J.W. (1990) Amplification and direct sequencing of fungal ribosomal RNA genes for phylogenetics. In *PCR Protocols: A Guide to Methods and Application*. New York: Academic Press, Inc.

Zuccaro, A., Summerbell, R.C., Gams, W., Schroers, H.J., and Mitchell, J.I. (2004) A new *Acremonium* species associated with *Fucus* spp., and its affinity with a phylogenetically distinct marine *Emericellopsis* clade. *Stud Mycol* **50**: 283-297.

Table 1 Average abundances of bacteria and viruses, and the virus to bacterium ratio (VBR) for the sampled areas ("core", "ring in", "ring out", "outside", and "mat") at two depths (0 - 1 and 1 - 2 mm), in November and July. n.d. = not determined. Significant differences between the seasons, depths and sampled areas are noted by different lower case letters for both bacterial and viral abundances, and for the VBR.

	Bacteria (x 10^{10} g^{-1})		**Viruses (x 10^{10} g^{-1})**		**VBR**	
	November	**July**	**November**	**July**	**November**	**July**
Core 0 - 1 mm	1.0 ± 0.5^{a}	1.5 ± 0.4^{a}	3.0 ± 0.9^{a}	3.2 ± 0.5^{a}	2.9 ± 1.0^{a}	2.2 ± 0.4^{b}
Core 1 - 2 mm	0.9 ± 0.2^{b}	0.5 ± 0.3^{c}	2.9 ± 0.5^{b}	1.0 ± 0.7^{c}	3.2 ± 0.9^{a}	1.7 ± 0.3^{c}
Core	1.0 ± 0.4	1.1 ± 0.6	3.0 ± 1.1	2.2 ± 1.3	3.0 ± 1.0	2.0 ± 0.4
Ring in 0 - 1 mm	n.d	1.0 ± 0.4^{a}	n.d	2.7 ± 1.0^{a}	n.d	2.8 ± 0.7^{b}
Ring in 1 - 2 mm	n.d	0.5 ± 0.3^{c}	n.d	1.0 ± 0.6^{c}	n.d	2.2 ± 0.5^{c}
Ring in	n.d	0.7 ± 0.4	n.d	1.8 ± 1.2	n.d	2.5 ± 0.6
Ring out 0 - 1 mm	n.d	1.2 ± 0.4^{a}	n.d	3.6 ± 1.3^{a}	n.d	2.9 ± 0.7^{b}
Ring out 1 - 2 mm	n.d	0.4 ± 0.1^{c}	n.d	0.8 ± 0.4^{c}	n.d	2.1 ± 0.5^{c}
Ring out	n.d	0.8 ± 0.5	n.d	2.2 ± 1.6	n.d	2.5 ± 0.7
Outside 0 - 1 mm	1.3 ± 0.3^{a}	1.3 ± 0.2^{a}	3.7 ± 1.3^{a}	2.5 ± 0.8^{a}	3.1 ± 0.7^{a}	2.0 ± 0.4^{b}
Outside 1 - 2 mm	0.9 ± 0.3^{b}	0.4 ± 0.1^{c}	2.0 ± 1.7^{a}	0.8 ± 0.4^{c}	2.4 ± 1.8^{a}	1.7 ± 0.3^{c}
Outside	1.1 ± 0.3	0.9 ± 0.5	2.9 ± 1.5	1.9 ± 1.2	2.8 ± 1.3	1.9 ± 0.4
Mat 0 - 1 mm	n.d	1.4 ± 0.4^{a}	n.d	3.7 ± 1.3^{a}	n.d	2.6 ± 0.8^{b}
Mat 1 - 2 mm	n.d	0.4 ± 0.2^{c}	n.d	0.7 ± 0.4^{c}	n.d	2.0 ± 0.3^{c}
Mat	n.d	0.9 ± 0.6	n.d	2.3 ± 1.8	n.d	2.3 ± 0.7
Average 0 - 1 mm	1.1 ± 0.4	1.3 ± 0.4	3.3 ± 1.2^{a}	3.2 ± 1.0^{a}	3.0 ± 0.8	2.5 ± 0.7
Average 1 - 2 mm	0.9 ± 0.3	0.4 ± 0.2	2.5 ± 1.3^{b}	0.8 ± 0.5^{c}	2.8 ± 1.5	2.0 ± 0.4
Total Average	1.0 ± 0.4	0.9 ± 0.5	2.9 ± 1.3	2.1 ± 1.4	2.9 ± 1.2	2.3 ± 0.6

Table 2 Diameter, maximum expansion of rings after 10 days, and rate of expansion for rings 1 - 4 in November, and rings 5 - 8 in July.

Ring	Diameter (cm) day 0	Maximum expansion of infected area (cm)	Expansion rate (cm d^{-1})
1	4.20 ± 0.15	0.99 ± 0.18	0.10 ± 0.02
2	4.64 ± 0.32	1.05 ± 0.40	0.12 ± 0.04
3	2.23 ± 0.22	1.45 ± 0.10	0.16 ± 0.01
4	4.82 ± 0.49	1.57 ± 0.26	0.17 ± 0.03
5	3.07 ± 0.12	0.91 ± 0.09	0.09 ± 0.01
6	3.14 ± 0.13	1.08 ± 0.05	0.11 ± 0.01
7	2.58 ± 0.21	1.18 ± 0.22	0.13 ± 0.19
8	2.09 ± 0.30	1.00 ± 0.05	0.10 ± 0.01

538 **Figure Legends**

539

540 **Figure 1** Examples of blue to amber ratio (BAR) of the photosynthetic microbial mats.
541 Values < 0 indicate cyanobacteria dominance and values > 0 indicate diatom dominance.
542 (A) examplifies a microbial mat dominated by cyanobacteria, whereas (B) shows a mat of
543 mixed populations of cyanobacteria and diatoms.

544

545 **Figure 2** View of sampling area and examples of ring-like structures in photosynthetic
546 microbial mats on the Wadden Sea island Schiermonnikoog (The Netherlands), illustrating
547 the different environmental conditions in November (A, B) and July (C, D). Scale bar is the
548 same for B and D.

549

550 **Figure 3** Images and plot of autofluorescence across a ring structure. (A) Standard colour
551 camera image of a ring-like structure labelled with the different areas sampled: ring core
552 (core), inner ring (ring in), outer ring (ring out), outside near the ring (outside). (B)
553 Magnified colour image showing the ring-in and ring-out areas (white area contains most
554 fungal biomass), (C) autofluorescence (relative units) after amber excitation, (D)
555 autofluorescence (relative units) after blue light excitation of a ring structure; (E)
556 autofluorescence (relative units) dynamics after amber and blue light excitation across a
557 ring.

558

559 **Figure 4** The phylogenetic position of strain *Emericellopsis* sp. CBS 137197 within
560 Emericellopsis-clade based on partial sequences for ITS and β-tubulin analyzed by

maximum likelihood. The classification of Emericellopsis-clade in terrestrial clade, marine clade and soda soil clade was purposed by Grum-Grzhimaylo et al (2013).

Figure 5 Autofluorescence (relative units) (A, B, D, E) images after amber (A, D) and blue (B, E) light excitation, and colour images (C, F) of the infection of microbial mat with live (A - C), and killed (D - F) *Emericellopsis* sp. after 7 days of inoculation. Pipette tips were used to indicate inoculation sites. Arrows indicate the development of ring-like structures in the mat inoculated with live fungus.

Figure 6 Aufluorescence (relative units) images after amber (A - E) and blue (F - J) light excitation of the transplantation of a piece (1 x 0.5 x 0.1 cm indicated by the white square) of infected photosynthetic microbial mat into a non-infected microbial mat. Images collected at day 0 (A,F), 1 (B,G), 3 (C,H), 5 (D,I), and 7 (E,J). White rectangle indicates transplanted part, wherein the black area represents fungus-infected mat. The dark section below the transplanted part was a section without mat (only sediment). The white line (in and outside the rectangle) indicates the expansion of the fungus-infected area. Values (0 to 3) in colour scale indicate increasing autofluorescence of photoautotrophs.

Figure 7 Temporal development of a ring by colour imaging (A - D), and autofluorescence imaging after amber (E - H) and blue (I - L) light excitation. Autofluorescence images were made by overlapping autofluorescence image at day 0 with image at days 1 (E, I), 3 (F, J), 6 (G, K), and 10 (H, L). Values above 1 show growth in relation to day 0. Scale bar is 1 cm.

585 **Figure 8** Representation of the development of a ring structure. Initially a photosynthetic
586 microbial mat is infected with the fungus and develops the “ring in” area by degrading the
587 photoautotrophic mat. The fungus starts to attack the nearest non-infected mat creating
588 the “ring out” area. As the infection spread towards the outside, re-colonisation by diatoms
589 takes place in the newly available areas left behind. Cyanobacteria follow diatoms
590 colonisation and dominate the mat.